Pramana – J. Phys. (2022) 96:71
https://doi.org/10.1007/s12043-022-02333-y

Neutron spectrum reconstruction for liquid organic scintillators in low information scenarios via genetic algorithm

IAN HALVIC and SHIKHA PRASAD*

Department of Nuclear Engineering, Texas A&M University, 423 Spence St., College Station, TX77843, USA
*Corresponding author. E-mail: shikhap@tamu.edu

MS received 3 June 2021; revised 3 November 2021; accepted 15 December 2021

Abstract. Construction of neutron energy spectrum is of interest in various scientific fields such as nuclear power, nuclear security, industrial applications of nuclear and fundamental physics. A genetic neutron spectrum unfolding method is proposed to generate neutron energy spectrum giving light output data from a liquid organic scintillation detector. The method presented attempts to unfold given minimum *a priori* data, specifically it does not require an initial guess spectrum to be supplied. Two response matrices corresponding to an EJ-309 organic liquid scintillator are constructed for testing, with one matrix using the traditional discretisation and the other using an alternate discretisation based on the energy-to-light conversion process. Test cases include MCNPX-PoliMi simulated ^{252}Cf, AmLi and AmBe spectra with corresponding detector responses. The genetic method can perform a coarse unfolding of the test spectra, potentially enough to perform an initial categorisation of the spectra. Promising results are obtained when genetic method is used in conjunction with the existing MAXED unfolding code, which operates on the maximum entropy principle. In this scenario, accuracy appears to exceed MAXED using its built-in default *a priori* spectrum. The ^{252}Cf test case saw a reduction in the unfolded spectrum error from 5.08×10^{-3} to 9.42×10^{-5}. The AmLi and AmBe test cases could not be unfolded by MAXED using its default spectrum; however, when supplied with the genetic method result, MAXED could complete a successful unfold.

Keywords. Neutron unfolding; artificial intelligence; organic scintillation detectors; isotope identification.

PACS Nos 29.30.Hs; 28.60.+s; 29.40.Mc

1. Introduction

Liquid organic scintillation detectors offer a unique tool for researchers across multiple disciplines such as nuclear power, nuclear security, nuclear medicine, industrial applications of nuclear and fundamental physics. In particular, these detector systems can detect both fast neutron and gamma radiation using interactions occurring over nanosecond time frames as well as discriminate between incident radiation types. Recently, these detectors have found use in the fast neutron coincidence collar (FNCL) developed by the International Atomic Energy Agency to overcome limitations of detection focussed on moderated neutrons [1]. For fast neutron detection, the primary method of detection is the elastic scattering with hydrogen nuclei, in which the resulting energy deposition within the detector material is converted to detectable light. However, this method of detection presents a difficult problem: the energy transferred to the detector varies strongly with the scattering angle and therefore the energy of the observed light output cannot be easily translated back to the incident neutron energy. This problem of spectral reconstruction is termed as 'spectrum unfolding'. Spectrum unfolding often presents itself as a computationally hard problem, in which the algebraic formulation presents an ill-conditioned or even ill-posed system tasked with solving a linear system with more unknowns than the equations present.

Spectrum unfolding methods have their roots in Bonner sphere spectroscopy (BSS), in which the detector output is the total counts from individual moderated sphere detectors. Many methods have been adapted to organic liquid scintillators, in which the detector output is discretised by the detectable light energy. Despite the fundamental difference in these detector systems, they can often be modelled quite similarly.

Published online: 07 April 2022

2. Background

The field of spectrum unfolding has seen a wide variety of computational methods. The FORIST [2] and FERDOR [3] unfolding codes present early development in the field, singular value decomposition (SVD) methods offer a powerful tool for this field of research [4–6], while methods such as likelihood maximisation offer yet another approach [7] and Bayesian treatments present a well performing recent approach to the unfolding problem [8]. The primary differentiation between unfolding methods arises from their treatment of *a priori* data. A common *a priori* requirement is an initial approximation of the spectra to be supplied by the user. In scenarios where a user has a general idea about the composition or origin of a source, this *a priori* requirement may be reasonable. However, situations may arise in which the user has little or no information about the source in question. Then this *a priori* requirement becomes a limiting factor. The MAXED [9,10] and GRAVEL [11] iterative unfolding methods are examples of this. As an alternative, data-driven methods, such as artificial neural networks, have been explored to perform unfolding using data from previous measurements [12–14]. These data-driven methods are potentially powerful. However, the dataset frequently requires many measurements of known spectra which can be difficult to build and may not be available in all scenarios. Heuristic methods can be formulated which attempt to unfold without an initial spectrum, possibly only assuming positivity of the unfolded spectrum. Genetic algorithms in particular have shown some promise of unfolding and are the primary focus of this work [15–20].

The method presented in this work intends to refine and improve a previous genetic algorithm-based unfolding method developed by Halvic and Prasad [21]. The method presented incorporates fundamental changes to the underlying population to allow the method to better refine spectral features of varying magnitude along with alterations to the mutation method and implementation improvements allow for the use of more generations within a reasonable computation time (less than 5 min). Beyond the development of an unfolding method, two other related aspects are tested in this work. The first is an alternative discretisation of the response matrix used for unfolding, which relies on unique aspects of scintillation detection. The second aspect is on utilising the heuristic method presented here as a preprocessor to fulfill the *a priori* requirement for more widely used iterative methods. In particular, the genetic method developed in this work in conjunction with the existing MAXED unfolding code is considered.

2.1 *Response matrix formation*

Conceptually, the physics of the detection process can be divided into three steps. The first step is to determine the interactions between the neutrons and the detector, in particular the neutron elastic scattering reaction rate with protons within the scintillating material. A variety of neutron transport solvers, including MCNPX-PoliMi [22], are capable of accomplishing this. The second step maps these interactions into proton recoil energies within the material. In the case of elastic scattering, this can be carried out using the equations for conservation of momentum and energy. The final step translates the energy deposited in the material into the light pulses $c(L)$ observed by the detector's measurement system. The strengths of these light pulses are assigned an energy-equivalent $MeVee$ value through detector calibration. This conversion process can be driven by experimentally determined models for energy to light conversion, typically referred to as the energy-to-light function $g(E)$.

The formulation of the folding process can be presented in its continuous form as a Fredholm integral equation of the first kind, in which a kernel $K(L, E)$ representing the detector properties (including geometry, interaction rate, energy deposition and light production) is integrated with the continuous area integrated neutron current $J^+(E)$ to form a continuous detector response $c(L)$ [4].

$$c(L) = \int_0^\infty K(L, E) J^+(E) \mathrm{d}E. \tag{1}$$

The frequently employed response matrix method (RMM) represents a discretisation of eq. (1) by binning of both the neutron energy spectrum and the detector output. The detector output is discretised into a histogram of bins defined by points $\{L_0, ..., L_m\}$ and represented as an m length vector $\vec{c}$. Often $\{L_0, ..., L_N\}$ arises naturally from the counting method of the detector system and calibration. Similarly, the neutron energy spectrum is discretised into bins $\{E_0, ..., E_m\}$ and represented by the discretised area integrated neutron current $\vec{J}$. The detector is then modelled by the $m \times n$ response matrix $\mathbf{A}$ and eq. (1) assumes the discretised form

$$\vec{c} = \mathbf{A}\vec{J}\,. \tag{2}$$

In the context of liquid scintillation detectors, a common and expedient method for response matrix generation is to form the response matrix column-by-column using simulation software. A simulated source δ_j with all the initial energies within a single energy bin j is input into the software and the output detector response $\hat{c}_j$ is recorded as the jth column of $\mathbf{A}$. A

summation along each column of **A** gives the intrinsic efficiency of the detector [23].

$$\mathbf{A} \equiv \begin{bmatrix} \uparrow & & \uparrow \\ \hat{c}_0 & \cdots & \hat{c}_{m-1} \\ \downarrow & & \downarrow \end{bmatrix}, \quad \hat{c}_j = \text{Detect}(\delta_j). \tag{3}$$

While the discretisation of the detector output is still a result of the counting system, the use of simulation software presents a greater degree of freedom to the researcher in choosing the spectrum energy bins. Frequently, the energy bins are chosen using an equal spacing of bins. Functionally this allows a researcher to have fine control over the resolution of the unfolded energy spectrum. In this work, an alternative discretisation is tested based on energy conservation. An inverse of the energy-to-light function $g^{-1}(L)$ is formulated and applied to the output light bins, resulting in the energy discretisation shown in eq. (4). Because the pulse bins are calibrated to an energy equivalent $MeVee$, conservation of energy implies that in the response matrix construction, Detect(δ_j) yields $p_i = 0$ for $i > j$.

$$\{E_0, ..., E_{n=m}\} \equiv \{g^{-1}(L_0), ..., g^{-1}(L_m)\}. \tag{4}$$

The result of this construction is a square response matrix with a specific sparsity pattern defined by the detector physics and is shown in figure 1. Region I is the sparse lower triangular region representing light output bins which are not energetically possible due to the discretisation described in eq. (4). Region II is the result of the lower limit of the detector, where all the light pulses below the L_{LO} threshold are not detected by the detector's photodetection system. This may be the result of a physical lack of interaction or by falling below the detector's voltage threshold. Because this represents interactions of such low emission, they produce no response at all and this region can be truncated from the response matrix by setting $L_0 = L_{LO}$ and thus $E_0 = g^{-1}(L_{LO})$. Region III presents a more problematic sparse region representing high-energy light pulses that cannot be observed by the detector. Once again, this may be the result of physical interaction or an overvoltage in the detector system. In contrast to region II, this region cannot simply be truncated because these high-energy neutrons still induce response in lower-energy light channels due to more glancing scattering angles. The remaining region IV remains populated. This construction relies on the assumption that $g(E)$ is monotonically increasing, which is the case for EJ-309-based neutron detectors within the energy ranges of interest [24,25]. The most obvious consequence of this construction is that the energy bins are now generally of unequal width, and this construction is termed as the 'variable width' response matrix for this work. For the $g(E)$ function used in subsequent section $\mathrm{d}^2g/\mathrm{d}E^2 > 0$, which results in energy bins becoming narrower at higher energies.

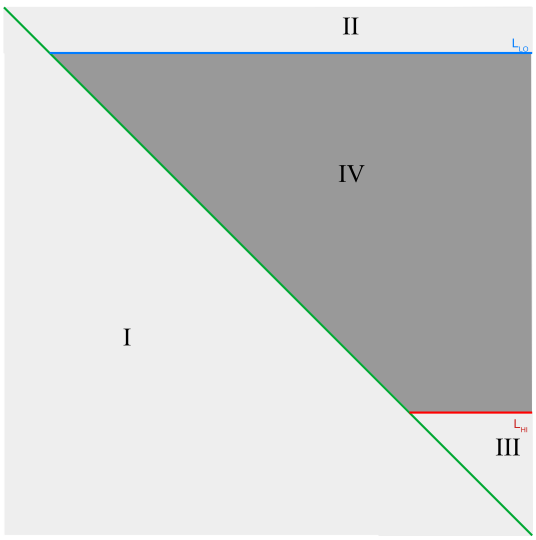

Figure 1. Response matrix sparsity diagram. Non-zero entries are shaded. Region I is zero due to the discretisation based on $g(E)$. Regions II and III are zero because the interactions fall below or above the detector's lower and upper thresholds respectively. Region IV models the detectable interactions occurring within the detector system. Diagonal L_{LO} and L_{HI} are shown for reference.

3. Genetic algorithm

Genetic algorithms represent an optimisation method inspired by natural evolution. Initially, a collection of potential solutions is generated by some computationally efficient method. To reflect the biological nature of the method, each potential solution is called an 'individual', whereas the collection of the individuals is called a 'population'. Within the population, each individual is assigned a fitness value based on how well it solves the problem at hand. An iterative process then begins in which individuals from the population are randomly selected and mated to produce the next generation of individuals. The mating selection process occurs in such a way that more fit individuals are more likely to be selected for mating and have their traits expressed in the next generation. To maintain diversity within the population, a mutation method is often implemented that can cause random, spontaneous and possibly drastic changes within the individuals. This generational evolutionary process continues until some threshold is achieved, whether it be a certain level of fitness or a maximum number of generations achieved. On a practical note, genetic methods often allow for fairly simple form of parallelism by evolving multiple isolated or

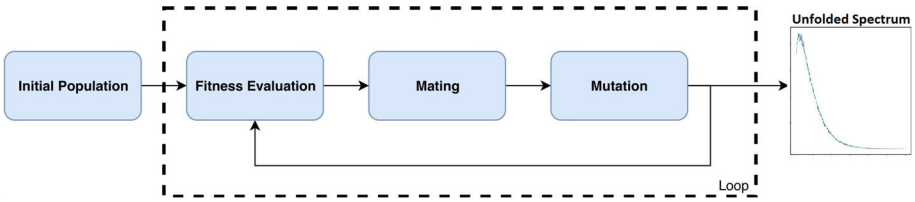

Figure 2. Genetic algorithm loop. An initial population is generated, at which point it iterates through generations by mating individuals based on their relative fitness to produce subsequent generations. Mutation events occur with a small probability in each generation to maintain genetic diversity. Through successive generations, individuals are expected to become more and more fit. The most fit final individual represents the unfolded spectrum.

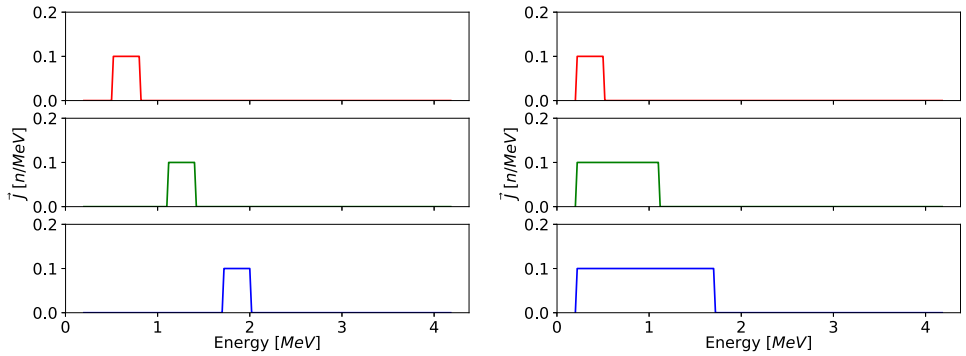

(a) Type1 (b) Type2

Figure 3. Three members of each initial population type for comparison. Type 1 are blocks within individual energy bins. Type 2 are blocks of varying width starting at E_0.

semi-isolated populations separately, and these are often referred to as islands (figure 2).

For the unfolding method presented in this paper, an individual within the population represents an unnormalised predicted neutron current spectrum. The notation $\vec{J}^{(g,t)}$ denotes the tth individual of the gth generation. Normalisation occurs via a scaling factor α used to equate the total light pulses of the folded individual and the total light pulses in the observed detector output. After the final generation $g = G$, the ultimately returned value is $\alpha^{(G,\text{opt})}\vec{J}^{(G,\text{opt})}$, where $\vec{J}^{(G,\text{opt})}$ represents the most fit individual within the final generation.

$$\alpha^{(g,t)} \equiv \frac{||\vec{c}||_1}{||\mathbf{A}\vec{J}^{(g,t)}||_1}. \tag{5}$$

3.1 *Errors and fitness*

Genetic fitness within the method is driven by the underlying metric ϵ_c, which quantifies how close the folded approximated spectrum is to the observable detector light output.

$$\epsilon_c^{(g,t)} \equiv \frac{||\alpha^{(g,t)}\mathbf{A}\vec{J}^{(g,t)} - \vec{c}||_1}{||\vec{c}||_1}. \tag{6}$$

For each member of a generation, its fitness is how well it minimises ϵ_c, relative to the worst performing member of the population (the most fit individual is the one with the lowest ϵ_c value).

$$f^{(g,t)} \equiv \max_{\hat{t}}(\epsilon_c^{(g,\hat{t})}) - \epsilon_c^{(g,t)}. \tag{7}$$

3.1.1 *Initial population.* The initial population members $\vec{J}^{(0,t)}$ are defined using two types of 'blocks' within the unfolded spectrum space. The Type 1 blocks represent simple elements that make little assumption about the target spectrum. The Type 2 blocks are of varying width and may allow for quicker convergence for spectra biased towards lower energies (figure 3).

$$\text{Type 1: } \vec{J}^{(0,t)} = \begin{cases} h, & E_{t-1} \le E < E_t \\ 0, & \text{else} \end{cases} \tag{8}$$

$$\text{Type 2: } \vec{J}^{(0,t)} = \begin{cases} h, & E_0 \le E < E_t \\ 0, & \text{else} \end{cases} \tag{9}$$

3.1.2 *Mating method.* Mating selection probability P_s is driven by an individual's fitness value using a fitness proportionate selection $P_s(\vec{J}^{(g,t)}) = f^{(g,t)}/\sum_{\hat{t}}(f^{(g,\hat{t})})$, which causes more fit individuals to be selected more often for mating. Upon selection of two parent solutions $\vec{J}^{(g,P1)}$, $\vec{J}^{(g,P2)}$, two children $\vec{J}^{(g+1,C1)}$, $\vec{J}^{(g+1,C2)}$ are generated for the next generation through a simple linear

combination. The choice of ± differentiates $\vec{J}^{(g+1,C1)}$ from $\vec{J}^{(g+1,C2)}$. Coupled with the block-like form of the initial population, the mating process represents a 'stacking' of successive generations in an attempt to reproduce the target energy spectral shape.

$$\vec{J}^{(g+1,\{C1,C2\})} = \vec{J}^{(g,P1)} \pm \vec{J}^{(g,P2)}. \tag{10}$$

In addition to the individuals produced via mating, the most fit individual from the parent's generation is carried over unchanged to the next generation. This action guarantees that the returned most fit individual of the final generation is the most fit individual found within all generations.

3.1.3 *Mutation.* After mating has occurred for a generation, each offspring undergoes a mutation with probability P_m. During a mutation event, an individual $\vec{J}^{(g,t)}$ is mutated by zeroing the corresponding spectrum above or below a randomly chosen energy bin E_r. The choice of zeroing direction is the result of an unbiased coin flip. The resulting mutated individual $\vec{J}^{(g,m)}$ replaces $\vec{J}^{(g,i)}$ within the population.

$$\vec{J}^{(g,m)} = \begin{cases} \vec{J}^{(g,t)}, & E \leq E_r \\ 0, & E > E_r \end{cases}$$

OR

$$\vec{J}^{(g,m)} = \begin{cases} 0, & E \leq E_r \\ \vec{J}^{(g,t)}, & E > E_r \end{cases}. \tag{11}$$

3.1.4 *Complexity.* Time complexity of the genetic method outlined is dominated by the $\mathcal{O}(mn_k)$ folding operation of eq. (2) required to compute the fitness of each individual within each population of each generation. This leads to an overall complexity of $\mathcal{O}(PGmn_k)$ for a single run of the method, where P is the size of the population and G is the total number of generations the method is run for. Multiple independent runs of the method can be executed in parallel and final results can be simply compared if desired.

3.1.5 *Coupling with MAXED.* Beyond using the genetic method described above as a complete unfolding method, it is potentially valuable as a preprocessor for methods which require more robust *a priori* data. In this scenario, the genetic method could be used to generate an approximate spectrum to then be used as an initial guess in other methods which require such input. To explore this application, the MAXED unfolding code was chosen to process the output of the genetic algorithm. The MAXED input files containing the light spectra and the energy-to-light response curves have been uploaded on GitHub for the interested reader. The light spectrum for all the three nuclides have been provided from 0.01 to 1.99 MeVee. These files can be accessed at: https://github.com/shikhaprasad/UnfoldingNeutronSpectra.

4. Results

MNCPX-PoliMi [26] coupled with the MPPost [22] post-processor was used to construct two response matrices corresponding to a cylindrical EJ-309 liquid scintillation detector with 127 mm diameter and 127 mm height. MPPost was run using an energy to light conversion modelled by $g(E) = 0.03495E^2 + 0.1424E - 0.036$ [23]. Both matrices discretised light output into 199 bins, and the corresponding light output from 0.01 to 2 MeVee in 0.01 MeVee intervals. The first response matrix used a fixed spacing of 0.02 MeV from 0.3 to 15 MeV for the neutron spectrum, resulting in a response matrix of 199 light bins by 735 energy bins. The second response matrix used the $g(E)$-based neutron bin widths discussed earlier, resulting in a response matrix of 199 light bins by 996 energy bins, with varying energy bin widths from 0.009 to 0.060 MeV.

Additionally, three test nuclides placed 30 cm from the detector were simulated using an MCNPX-PoliMi simulation with 10^8 neutron histories. These included a spontaneous fission ^{252}Cf source as well as AmBe [27] and AmLi [28] (α, n) emission sources. For each simulation, the light response in the detector was recorded along with a current (F1) tally measuring the area integrated current of the source emission spectrum to use as a reference solution for unfolding. As a verification of the RMM, the tallied spectra were folded using each of the generated response matrix and compared against the analog MCNPX-PoliMi responses as shown in figure 4. An agreement was shown between the simulated analog detector response and the RMM-produced response, though at higher energies the counting noise caused deviations, especially with the AmLi test case. Additionally, an integer factor k was introduced to test altering the binning structure by combining k neighbouring energy bins into a single energy bin. This factor functionally reduces the energy resolution of the unfolded spectrum, with an altered number of energy bins given by $n_k = \lceil n/k \rceil$. The reduction in energy resolution results in fewer bins for the unfolding method to solve for, generating an 'easier' problem.

The genetic algorithm described was then run on the three nuclide test cases. The program run parameters consisted of a 2001 member population evolved for 2000 generations with a mutation rate of $P_m = 0.05$. Discreitisation factors of $k = \{1, 2, 4, 8\}$ were tested to observe the effect of varying the number of energy bins

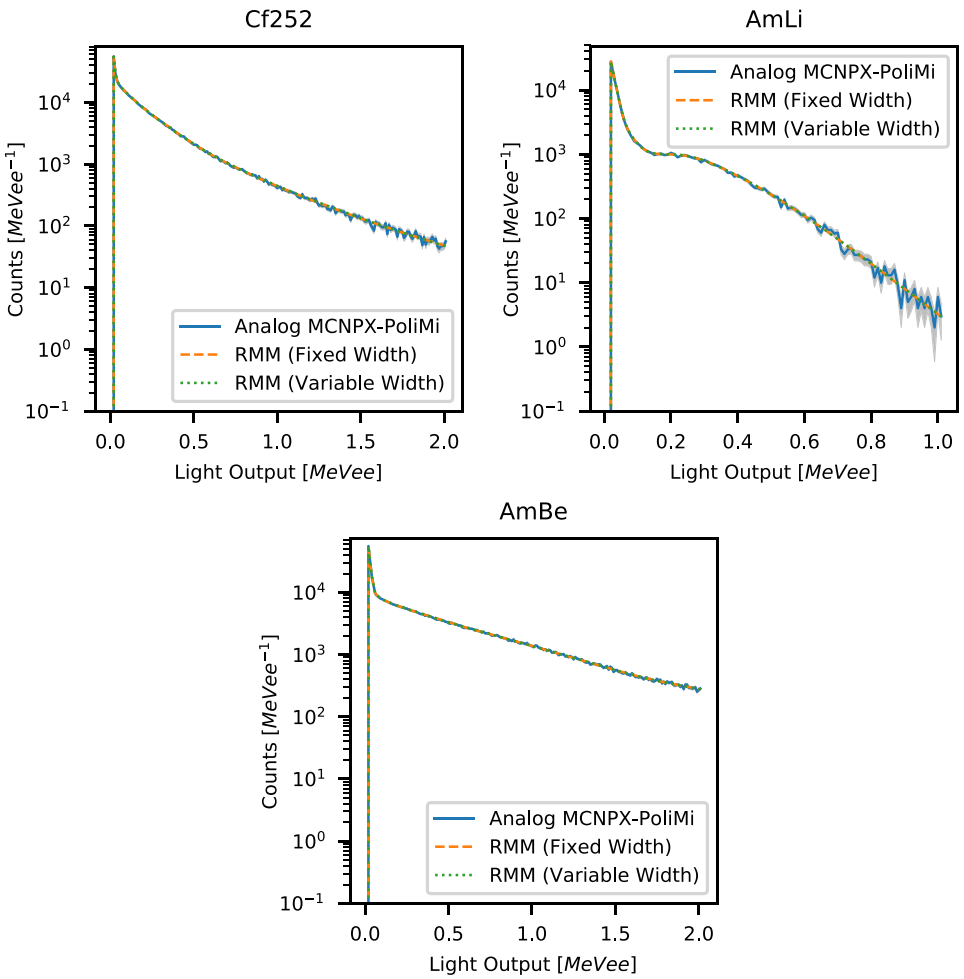

Figure 4. Comparison of analog MCNPX-PoliMi simulated detector response and the RMM from MCNPX-PoliMi combined with MCNPX neutron current results. Two separate response matrices were generated, each using a different neutron energy spectrum discretisation. An agreement is shown for low light energies. At higher light energies, counting statistics becomes more apparent and the RMM presents a smoothed solution which loses the apparent noisy behaviour. The AmLi source, due to its low-peaked neutron spectrum, experiences a more rapid drop off of counts at higher MeVee values and the x-axis is adjusted accordingly.

Table 1. Effect of the discretisation factor k on the energy bin structure. An increase in k corresponds to combining columns of the response matrix, reducing the number of energy bins to n_k and increase the width. For the variable width response matrix construction, the largest bin width and the smallest bin width are shown, corresponding to the lowest energy bin and highest energy bin respectively. Runtime is given in seconds per independent trial run.

	Fixed width response			Variable width response		
k	n_k	Width (MeV)	Sec/trial	n_k	Width (MeV)	Sec/trial
1	735	0.02	185	996	0.060 → 0.009	247
2	368	0.04	99	498	0.119 → 0.016	129
4	184	0.08	55	249	0.233 → 0.034	71
8	92	0.16	30	125	0.447 → 0.068	38

to solve for. Each combination of response matrix and k was repeated 128 times using varying random seeds to provide insight on the stochastic behaviour of the method. Table 1 shows the effect of n_k on the width of the unfolded energy bins as well as run time per trial executed on an Intel i5-7300HQ processor with 16 GB of

Table 2. Run metrics for 128 trials of the genetic method per test nuclide. Metrics presented include the average and best performing light output errors as well as the percentage of rejected trials corresponding to a spurious solution.

	Fixed width response								
	^{252}Cf			AmLi			AmBe		
k	$\epsilon_{c,\text{avg}}$	$\epsilon_{c,\text{min}}$	Rej (%)	$\epsilon_{c,\text{avg}}$	$\epsilon_{c,\text{min}}$	Rej (%)	$\epsilon_{c,\text{avg}}$	$\epsilon_{c,\text{min}}$	Rej (%)
1	0.1174	0.1113	14.8	0.3029	0.2774	21.1	0.1106	0.1067	11.7
2	0.1179	0.1119	7.8	0.3023	0.2784	8.6	0.1106	0.1066	11.7
4	0.1180	0.1116	0	0.3030	0.2774	0	0.1106	0.1054	0
8	0.1177	0.1112	0	0.3079	0.2775	0	0.1109	0.1058	0
	Variable width response								
	^{252}Cf			AmLi			AmBe		
k	$\epsilon_{c,\text{avg}}$	$\epsilon_{c,\text{min}}$	Rej (%)	$\epsilon_{c,\text{avg}}$	$\epsilon_{c,\text{min}}$	Rej (%)	$\epsilon_{c,\text{avg}}$	$\epsilon_{c,\text{min}}$	Rej (%)
1	0.1173	0.1106	5.4	0.3170	0.2796	5.5	0.1102	0.1052	2.3
2	0.1170	0.1107	0	0.3195	0.2788	0	0.1103	0.1062	0
4	0.1174	0.1117	0	0.3204	0.2816	0	0.1103	0.1066	0
8	0.1172	0.1123	0	0.3200	0.2793	0	0.1102	0.1054	0

system memory. Results of individual runs were evaluated by their relative error of the reconstructed response (ϵ_c). $\epsilon_{c,\text{avg}}$ represents the average error over 128 trials while $\epsilon_{c,\text{min}}$ represents the best fitting solution of 128 trials. An undesirable consequence of the stochastic nature are spurious solutions and local minimum traps. To account for such results, individual trials in which the output had a relative error $\epsilon_c > 100\%$ were given a zero weight when computing $\epsilon_{c,\text{avg}}$ and counted as 'rejected'. Run metrics are recorded in table 2. A noticeable difference between the response matrices used is that the variable width response matrix seemed to be more resistant to spurious results for low k values, even though the system had more neutron energy bins to be solved than the fixed width response matrix.

The selected unfolded spectra for all the test nuclides are shown in figure 5 with the MCNPX-generated spectrum as the reference. $k = 4$ was chosen for the selected results as this appeared to be the minimum k required to avoid rejected trials within the runs. Unfolding of the ^{252}Cf spectrum appeared to fare the best, capturing the general characteristics, albeit with the peak energy shifted towards higher energies. The test AmLi spectrum is dominated by a single low energy peak. This nature is somewhat reflected in the unfolded spectrum with a reduced magnitude, likely as a result of the coarsening of the unfolded spectrum resolution resulting from the k factor chosen. The unfolded AmBe spectrum performed very poorly and struggled to recreate the complex shape of the reference spectrum, with the best performing spectrum often falling outside the $\pm 1\sigma$ range found over 128 trials.

To test the use of the genetic method as a preprocessor, the predicted spectrum found using the genetic algorithm was then supplied as an initial guess to the MAXED unfolding code. We term this method GA→MAXED for brevity. The predicted spectrum supplied was chosen as the spectrum which most closely matched the observed light output after folding with the RMM. An uncertainty value was computed for the supplied spectrum by assuming 10^8 total counts and taking the square root, which is also utilised by MAXED. Additionally, unfolding using MAXED supplied with MAXED's built-in default flat spectrum as an initial guess was attempted for all test cases. However, only the ^{252}Cf test case converged when using this default initial guess. The AmBe test case could not resolve the solution further than the flat initial guess, and the AmLi test case simply errored. Comparison of the various solutions to the reference spectrum were made using two error metrics. A commonly used mean squared error (MSE) was applied. In addition, a spectral angle mapper (SAM) [29] was also applied to the results. SAM is based on the angle between two spectra in a high-dimensional space and focussed more on comparing the overall spectral shape as opposed to the magnitude of individual bins. The SAM metric runs from 0° to 180°, with 0° representing perfect alignment between the spectral shapes and the best possible fit according to this metric. These two error metrics, along with the average energy of all available spectra, are recorded in table 3.

$$\text{MSE} = \frac{1}{n}\sum_n (\vec{J}_{\text{ref}} - \vec{J}_{\text{pred}})^2 \tag{12}$$

$$\text{SAM} = \cos^{-1}\left(\frac{\vec{J}_{\text{ref}} \cdot \vec{J}_{\text{pred}}}{||\vec{J}_{\text{ref}}||_2 ||\vec{J}_{\text{pred}}||_2}\right) \tag{13}$$

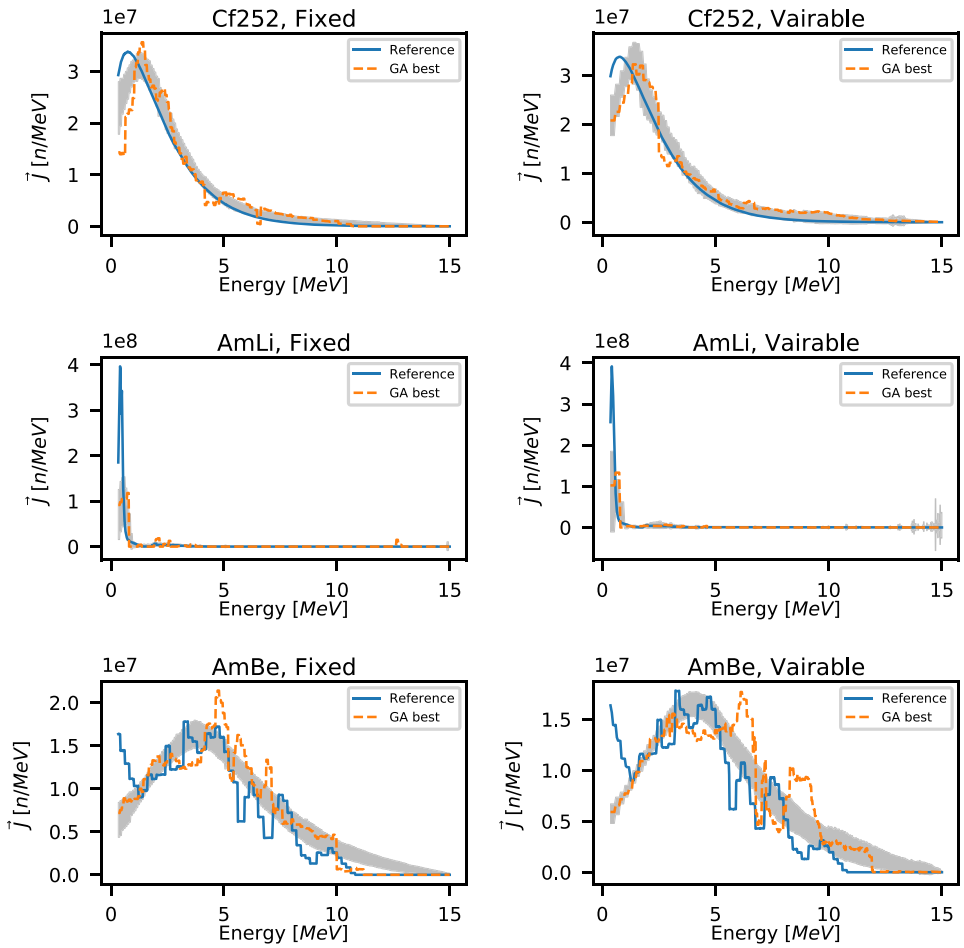

Figure 5. Plot shows the best solution obtained from the 128 individual runs of the genetic algorithm method, where the best is determined by the solution which minimises the error between the folded spectrum and the observed light output. The MCNPX-generated reference spectrum is shown for comparison. Results separated by nuclide and response matrix method used. The shaded region represents the mean and a $\pm 1\sigma$ range of the 128 runs, which helps in demonstrating the convergence of the GA method towards the true solution. In the case of AmBe, the reconstruction algorithm struggled and the best performing sprectrum fell outside the mean and the $\pm 1\sigma$ range.

Table 3. Comparison of unfolded spectra using the genetic method (GA), the MAXED unfolding code, and then using the genetic method as a preprocessor for MAXED (GA→MAXED). MCNPX-PoliMi F1 tally is used as the reference value. Expected neutron energy is provided, along with MSE and SAM error metric. Neither the AmLi or AmBe test cases were able to produce meaningful results using MAXED alone with its default initial spectrum.

		Fixed width response								
		E_{avg}			MSE			SAM		
Nuclide	F1	GA	MAXED	GA→MAXED	GA	MAXED	GA→MAXED	GA	MAXED	GA→MAXED
^{252}Cf	2.26	2.77	4.02	2.51	1.33×10^{-3}	5.08×10^{-3}	9.42×10^{-5}	17.8	36.7	4.7
AmLi	0.60	1.24	–	0.67	8.16×10^{-2}	–	3.47×10^{-2}	45.1	–	26.2
AmBe	4.16	4.62	–	4.87	7.90×10^{-4}	–	5.31×10^{-4}	17.5	–	14.7
		Variable width response								
		E_{avg}			MSE			SAM		
Nuclide	F1	GA	MAXED	GA→MAXED	GA	MAXED	GA→MAXED	GA	MAXED	GA→MAXED
^{252}Cf	2.26	3.04	4.00	2.41	9.00×10^{-4}	5.09×10^{-3}	2.15×10^{-4}	14.6	36.7	5.8
AmLi	0.60	0.85	–	0.99	7.85×10^{-2}	–	1.16×10^{-1}	45.5	–	51.6
AmBe	4.16	5.07	–	4.59	1.31×10^{-3}	–	4.17×10^{-4}	23.1	–	12.7

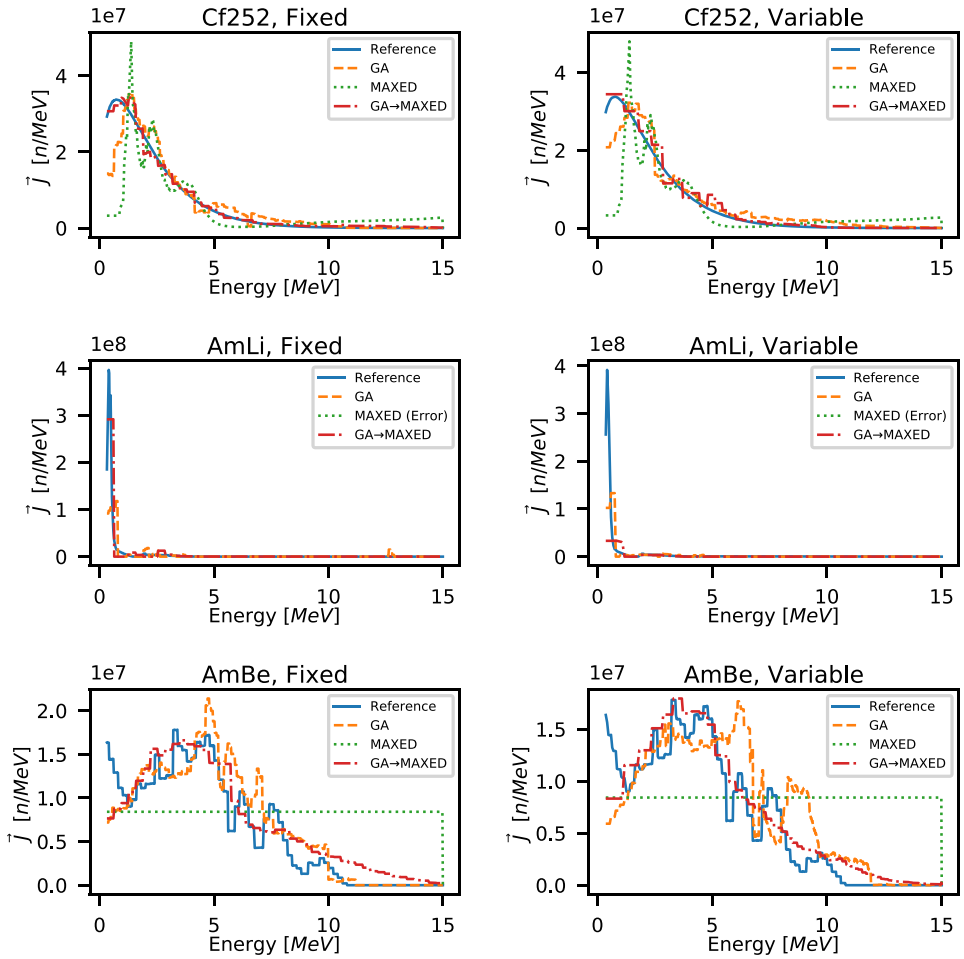

Figure 6. Comparison of three unfolding methods. MAXED using the default flat spectrum (when available), the genetic algorithm found result, and the unfold using the genetic found result as the prior spectrum for MAXED.The MCNPX spectrum is shown for reference. Results are separated by nuclide and the type of response matrix method used. MAXED failed to run for the AmLi test case using the default flat prior, and produced an error.

Unfolding performance was evaluated using a combination of the metrics presented in table 3 and inspection of the unfolded spectra is presented in figure 6. The unfolded ^{252}Cf spectrum using GA→MAXED outperformed both MAXED and the genetic method operating on their own according to selected metrics. Notably, the MSE error dropped from 5.08×10^{-3} using MAXED alone to 9.42×10^{-5} when using GA→MAXED. Additionally, the resulting spectrum was visually more similar to the reference spectrum. Inspection of the AmLi results showed significant improvement in E_{avg} (1.24 MeV → 0.67 MeV) and SAM (45.1 → 26.2) as well as mild improvement in MSE (8.16×10^{-2} → 3.47×10^{-2}) when GA → MAXED was used with the fixed width response matrix. However, when GA → MAXED was applied using the variable width response matrix, the result was in a degradation of accuracy in all three metrics. Examination of the plotted spectrum showed broadening of the dominant low-energy peak of the spectrum, which was the likely cause for the worse performing metrics in this case. For the AmBe test case, applying GA→MAXED with the fixed width response resulted in a small improvement in error metrics, though there was a shift in the E_{avg} value away from the reference value. Unfolding of AmBe with GA→MAXED using the variable width response resulted in similar error metrics to the fixed width test, but also showed improvement in E_{avg}. Visual inspection of the unfolded AmBe spectra shows that application of GA→MAXED gives a somewhat smoothed spectrum which still does not fully capture some of the more complex structures within the reference spectrum, though the overall shift in the spectra appears to better align with the reference.

5. Conclusions

The genetic algorithm for neutron spectrum unfolding formulated for organic scintillation detectors within this work showed promising results. In a scenario in which a researcher is faced with an unknown neutron source and is unable to determine an initial guess spectrum required for many unfolding methods, the genetic unfolding method can produce a coarse approximation of the spectral shape. Unfolding of a ^{252}Cf test spectrum with the genetic method performed well resulting in a spectrum reasonably identifiable as a fission spectrum, although the expected neutron energy is shifted to 2.77 MeV compared to 2.26 MeV from the reference. Unfolding performance is further improved by using the GA→MAXED method, in which case the MSE of using the codes combined (9.42×10^{-5}) outperformed the individual use of either the genetic method (1.33×10^{-3}) or MAXED operating under similar *a priori* information (5.08×10^{-3}). Results were more mixed with AmLi and AmBe test cases. For both AmLi and AmBe , MAXED was unable to produce a meaningful solution using its built-in default spectrum (AmBe returned the flat default spectra and AmLi resulted in an error). The reference AmLi spectrum is dominated by a low-energy peak which has a significant impact on the expected neutron energy. Using GA→MAXED resulted in an expected neutron energy of 0.67 MeV which agrees quite well with the reference spectrum of 0.60 MeV expected energy. The AmBe test spectrum represented a fairly complex spectrum to unfold. Applying GA→MAXED to the AmBe spectrum resulted in an unfolded spectrum that gave a visually smoothed version of the reference spectrum which lacked some of the finer spectral details expected but saw a reduction in MSE compared to using the genetic method alone (7.90×10^{-4} to 5.31×10^{-4}). This did cause a degradation in the prediction of the expected neutron energy, shifting from 4.62 to 4.87 MeV, compared to the reference 4.16 MeV. These coarse spectral approximations are potentially enough to inform the researcher of source properties to be used in determining the next steps towards identification or quantification.

Additionally, an alternate discretisation of the response matrix based on the energy conversion process was tested within the context of the genetic unfolding method. This alternate discretisation uses the energy-to-light function to generate a response matrix with a more structured sparsity pattern by using variable width energy bins. When used with the genetic unfolding method, this variable width response matrix appeared to better avoid spurious results with exceedingly high light output errors, compared to a more traditional fixed width response matrix. However, this generally comes at a cost of lower unfolding resolution at lower energies resulting in worse accuracy when compared to the fixed width results. For the AmBe test case, using this variable width response matrix with the GA→MAXED improved the performance slightly, resulting in an MSE of 4.17×10^{-4} and expected neutron energy of 4.5 MeV. In contrast, the effect of the undesirable low-energy resolution was most problematic for the AmLi test case, where the reduced folding resolution resulted in an undesirable broadening of the characteristic peak when used with the MAXED code, shifting the expected neutron energy away from the reference value to 0.99 MeV. This alternate construction could be explored using unfolding methods created to better exploit its structure in future work. Generally, methods need to be explored for low neutron energies where the unfolding problem is most complicated due to the underlying response matrix.

Acknowledgement

This research was supported by the Texas A&M Engineering Experiment Station.

References

[1] J Beaumont, T Lee, M Mayorov, C Tintori, F Rogo, B Angelucci and M Corbo, *J. Radioanal. Nucl. Chem.* **314**, 803 (2017)
[2] R Johnson and B Wehring, *FORIST unfolding code (ORNL/RSIC–40)* (1976)
[3] W Burrus and J Drischler, *The FERDOR unfolding code (ORNL-4154)* (1965)
[4] J Půpán and M Králík, *Nucl. Instrum. Methods Phys. Res. A* **325**, 314 (1993)
[5] A Höcker and V Kartvelishvili, *Nucl. Instrum. Methods Phys. Res. A* **372**, 469 (1996)
[6] D Stuenkel, J Holloway and G Knoll, *Nucl. Sci. Eng.* **132**, 261 (1999)
[7] B Pehlivanovic, S Avdic, P Marinkovic, S Pozzi and M Flaska, *Radiat. Meas.* **49**, 109 (2013)
[8] H Zhu, Y Altmann, A Fulvio, S McLaughlin, S Pozzi and A Hero, *IEEE Trans. Nucl. Sci.* **66**, 2265 (2019)
[9] M Reginatto and P Goldhagen, *Health Phys.* **77**, 579 (1999)
[10] M Reginatto, P Goldhagen and S Neumann, *Nucl. Instrum. Methods Phys. Res. A* **476**, 242 (2002)
[11] M Matzke, *Unfolding of pulse height spectra: The HEPRO program system (PTB-N-19)* (1994)
[12] R Koohi-Fayegh, S Green, N Crout, G Taylor and M Scott, *Nucl. Instrum. Methods Phys. Res. A* **329**, 269 (1993)

[13] S Avdic, S A Pozzi and V Protopopescu, *Nucl. Instrum. Methods Phys. Res. A* **565**, 742 (2006)
[14] H R Vega-Carrillo, V M Hernández-Dávila, E Manzanares-Acuña, G A M Sánchez, M P I de la Torre, R Barquero, F Palacios, R M Villafañe, T A Arteaga and J M O Rodriguez, *Radiat. Meas.* **41**, 425 (2006)
[15] B Mukherjee, *Nucl. Instrum. Methods Phys. Res. A* **432**, 305 (1999)
[16] D W Freeman, D R Edwards and A E Bolon, *Nucl. Instrum. Methods Phys. Res. A* **425**, 549 (1999)
[17] V Suman and P Sarkar, *Nucl. Instrum. Methods Phys. Res. A* **737**, 76 (2014)
[18] H Shahabinejad, S Hosseini and M Sohrabpour, *Nucl. Instrum. Methods Phys. Res. A* **811**, 82 (2016)
[19] R Sharma, S Nandy and S Bhattacharyya, *Pramana– J. Phys.* **66**, 1125 (2006)
[20] H Karahan and R Ozdemir, *Praman – J. Phys.* **91**, 42 (2018)
[21] I Halvic and S Prasad, *Genetic algorithm for spectrum reconstruction of neutron sources*, 60th Annual Meeting of the INMM (2019)
[22] E C Miller, S D Clarke, M Flaska, S Prasad, S A Pozzi and E Padovani, *J. Nucl. Mater.* **40**, 34 (2012)
[23] S Prasad, S D Clarke, S A Pozzi and E W Larsen, *Nucl. Sci. Eng.* **172** 78 (2012)
[24] A Enqvist, C C Lawrence, B M Wieger, S A Pozzi and T N Massey, *Nucl. Instrum. Methods Phys. Res. A* **715**, 79 (2013)
[25] M A Norsworthy, A Poitrasson-Rivière, M L Ruch, S D Clarke and S A Pozzi, *Nucl. Instrum. Methods Phys. Res. A* **842**, 20 (2017)
[26] S A Pozzi, E Padovani and M Marseguerra, *Nucl. Instrum. Methods Phys. Res. A* **513**, 550 (2003)
[27] International Organization for Standardization, *Reference neutron radiations – part 1: Characteristics and methods of production (ISO 8529)* (1989).
[28] R Weinmann-Smith, D Beddingfield, A Enqvist and M Swinhoe, *Nucl. Instrum. Methods Phys. Res. A* **856**, 17 (2017)
[29] F Kruse, A Lefkoff, J Boardman, K Heidebrecht, A Shapiro, P Barloon and A Goetz, *Remote Sens. Environ.* **44**, 145 (1993)